2348 #1

Lunch A. box

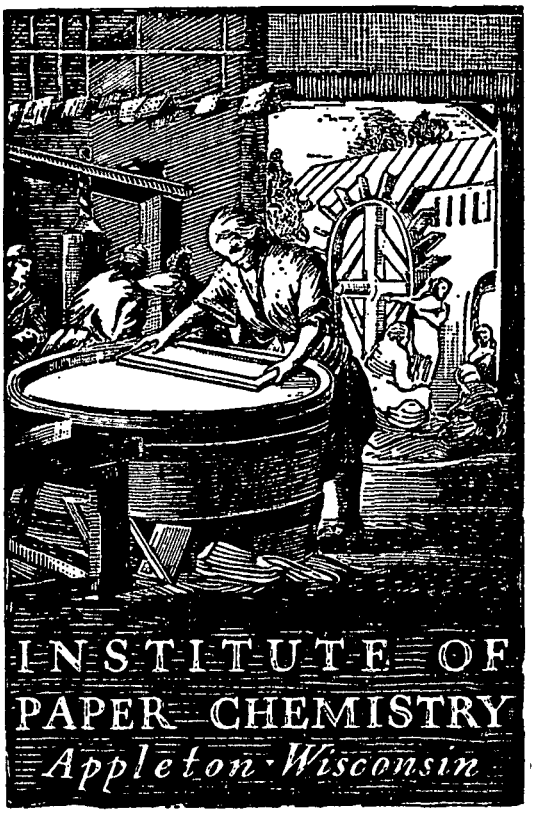

STUDIES OF THE SHEET-FORMING PROCESS

Dynamic Drainage

Project 2348

Report One

A Progress Report

to

MEMBERS OF GROUP PROJECT 2348

March 1, 1963

THE INSTITUTE OF PAPER CHEMISTRY
Appleton, Wisconsin

STUDIES OF THE SHEET-FORMING PROCESS

DYNAMIC DRAINAGE

Project 2348

Report One

A Progress Report to

MEMBERS OF GROUP PROJECT 2348

March 1, 1963

Members of Group Project 2348:

Consolidated Papers, Inc.
Crown Zellerbach Corporation
Eastman Kodak Company
The Eaton-Dikeman Company
P. H. Glatfelter Co.
International Paper Company
Kimberly-Clark Corporation
KVP Sutherland Paper Company
Longview Fibre Company
Marathon Division, American Can Company
The Mead Corporation
Personal Products Company
Riegel Paper Corporation
St. Regis Paper Co.
Scott Paper Company
Union Bag-Camp Paper Corporation
West Virginia Pulp & Paper Company

TABLE OF CONTENTS

THE INSTITUTE OF PAPER CHEMISTRY
Appleton, Wisconsin

STUDIES OF THE SHEET-FORMING PROCESS

DYNAMIC DRAINAGE

SUMMARY

The dynamic drainage tester capable of forming a sheet rapidly at a constant rate has been installed and calibrated. It consists of a vertical tube and a piston rigidly connected with a rack and pinion driving mechanism. The piston accelerates from rest to the driving speed well within 0.05 second and continues to oscillate about the mean speed with a small amplitude and at a major frequency corresponding to the gear teeth in the driving mechanism. The fluid pressure measured by a pressure transducer also fluctuates about a mean value at the same major frequency. The measurements of mean speed and pressure are reliable. At a piston speed of 100 cm. per sec. the sheet-forming time is about a second.

Initial sheet-forming tests were conducted with dacron fibers in dilute suspensions. The drainage results are in good agreement (within 10%) with the flow correlation previously established for permeation of mats of cylindrical fibers under equilibrium conditions. It is concluded from these experiments that for relatively incompressible fibers in dilute suspensions the drainage behavior and sheet structure in a forming time as low as 0.1 second remain the same as in slow filtrations of the order of 10 seconds. Subsequent tests will be given to highly compressible wood pulps to ascertain the possible presence of dynamic effects.

INTRODUCTION

The sheet-forming process has been treated as filtration, which is described to be the separation of fibers from a fluid by passing the fiber-fluid suspension through a wire screen. The elementary aspects of filtration have been studied under considerably simplified but clearly prescribed conditions, from which a rational picture and some useful information have emerged. The simple model cannot yet be used to predict drainage on a paper machine with a high degree of success. In the case of a fourdrinier machine, the actual drainage resistance has been found to be lower than the crude prediction by a factor of ten (1). This serious discrepancy must be resolved in order to attain some realistic understanding of the machine or "dynamic" drainage. Eventual clarification appears to come from two mutually dependent aspects of analysis: (1) the dynamic effects which have been neglected in the simple filtration theory, and (2) the known factors governing the filtration of a compressible mat, which have been ignored in the simple table-roll drainage theory (2, 3). This report deals with some preliminary investigations of the first aspect.

FILTRATION UNDER SIMPLIFIED CONDITIONS

Experimental and analytical studies of filtration have been made under the following idealized conditions:

1. Dilute Suspension

The fibers in the approaching suspension are randomly distributed in the space above the wire screen. They are free to move without forming flocs and to deposit on the screen without interference. To meet these requirements the suspension is made from purified water, deaerated for a length of time,

diluted to a low consistency in the neighborhood of 0.01%, kept agitated in the feed tank, and admitted to the filtration tube in a moderately turbulent flow.

2. Complete Retention

The retention of fibers is nearly complete at the very beginning of filtration by using a fine screen (100-150 mesh). If any loss of fibers occurs for an appreciable period of time, that portion of data is disregarded. The conditions of dilute suspension and complete retention are necessary to insure a uniform structure in the deposited layers of fibers.

3. Steady Flow

The filtration is carried out at a constant rate without appreciable flow pulsation. In early investigations the flow was confined to the viscous region, and has since been extended to the transition region up to a flow velocity of 300 cm. per sec. in permeation experiments.

4. Equilibrium Compressibility

The fiber mat being formed is assumed to respond instantaneously and reversibly to the fluid drag forces acting on the individual fibers. Under the equilibrium assumption only the local porosity of the mat changes with time; other features of the fiber structure, such as distributions of pore size and fiber orientation, remain unchanged during the whole filtration.

With the above simplifications the instantaneous drainage of a fiber mat is treated to be the same as permeation of fixed mats. The permeation equation is

$$\frac{\Delta P}{W/A} = \frac{\bar{k}(1 - \bar{\epsilon})vS_v^2\mu}{\bar{\epsilon}^3} U + \frac{b'\sqrt{\bar{k}}\, vS_v\rho}{\bar{\epsilon}^3} U^2 \qquad (1),$$

where

ΔP = pressure drop across the mat,

W/A = basis weight of the mat,

v = specific volume of the fiber,

S_v = specific surface of the fiber,

μ = viscosity of the fluid,

ρ = density of the fluid,

$$\bar{k} = k_1 \frac{\bar{\epsilon}^3}{(1 - \bar{\epsilon})^{1/2}} [1 + k_2(1 - \bar{\epsilon})^3] \qquad (2),$$

k_1 = 3.5, and k_2 = 57 for cylindrical fibers,

$$\bar{\epsilon} = 1 - (1 - \frac{N}{2})^2 vM(\Delta P)^N \qquad (3),$$

M and N being constants in the compressibility function for a mat of uniform porosity under the mechanical compacting pressure P,

$$1 - \epsilon = vMP^N \qquad (4),$$

and

b' = inertial resistance coefficient, 0.1 for cylindrical fibers.

To simplify the presentation of the experimental results, Correlation (1) is transformed into a dimensionless form:

$$\bar{f}' = \frac{\bar{\epsilon}^3 \Delta P}{\sqrt{\bar{k}}\, vS_v(W/A)\rho U^2} = \frac{\sqrt{\bar{k}}\,(1 - \bar{\epsilon})S_v\mu}{\rho U} + b'$$

$$= \frac{1}{\overline{Re}'} + b' \qquad (5).$$

Figure 1 shows this correlation in a logarithmic plot covering the range of $\overline{Re}'$ from 10^{-1} to 10^2 and $\bar{f}'$ from 10^{-1} to 10. The maximum deviation of a single point from the correlation is about $\pm 10\%$. The correlation was based on thick mats, and has since been extended to basis weights as low as 30 g. per sq. m.

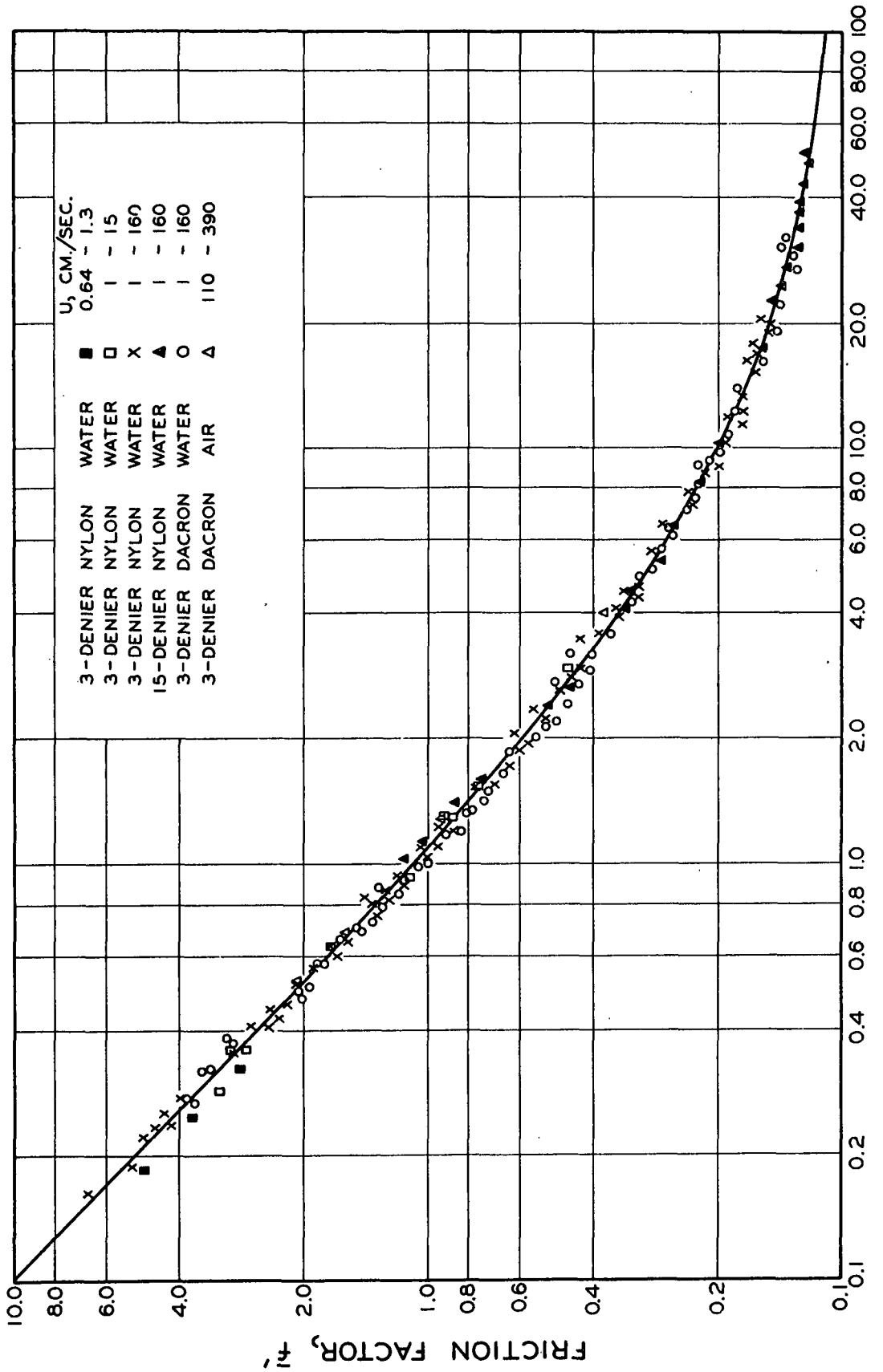

Figure 1. Correlation of Flow Through Mats of Cylindrical Fibers

While such a generalized correlation is simple in presentation and convenient for use, it tends to obscure any consistent trends of deviation in the neighborhood of experimental precision.

DYNAMIC EFFECTS

Having established a quantitative description of drainage, we proceed to ascertain the possible effects beyond the prescribed conditions of simple filtration. Drainage of high-consistency suspensions induces velocity gradients in the mat in the direction of flow. This added flow complexity is treated elsewhere (4). Incomplete retention results in the structural changes in the initial layers of fibers, causing anomalies in drainage. This aspect will be discussed in another report of this project on the permeation of thin mats.

The effects concerned here are primarily of the nonequilibrium nature, and are always associated with rapid changes or sometimes with cyclic variations. To simplify the discussion we restrict our considerations to filtrations of a dilute fiber suspension with complete retention.

1. Fluid Acceleration

When drainage of a fiber suspension is suddenly initiated by an external force (pressure difference), the fluid must undergo acceleration because of the unbalanced force acting on the system. The direction and magnitude of the acceleration is determined solely by the vector difference between the driving force and the frictional force responding to the drainage resistance which in turn is dependent on the flow velocity. A state of uniform motion (steady flow) will be reached when the two opposing forces balance each other.

If the acceleration is moderate, the system will be stable. However, with extreme accelerations the flow may become highly unstable. Hydrodynamic instability, such as surge or spouting at free surfaces, is under investigation in other laboratories, and will not be considered here.

The effects of fluid acceleration are twofold. In the first place, the fibers suspended in the fluid will also undergo acceleration. Since the dimensions of fibers are small compared with the fluid space and the fiber density is about the same as water density, the fibers will follow the motion of the fluid in normal flow of suspension. For a fiber of ordinary dimensions to accelerate to a velocity ten times its original velocity under viscous resistance, the time required is of the order of 10^{-4} sec. In the second place, the fibers arrested in the formed mat are subjected to changes of the drag force arising from fluid acceleration. The question often raised concerns the response of fibers in a mat to such compressive stresses.

2. Mat Response

When a wet mat of viscoelastic fibers supported on a solid plate is suddenly subjected to a compacting load of a permeable piston, its response of deformation is dependent on time. As shown by Wilder (5), the deformation of the mat as measured by fiber consistency increases rapidly in a short period and from there on creeps indefinitely.

The creep part of deformation is exponential as indicated by the slanting line in the following sketch, and may be attributed entirely to the viscoelasticity of fibers.

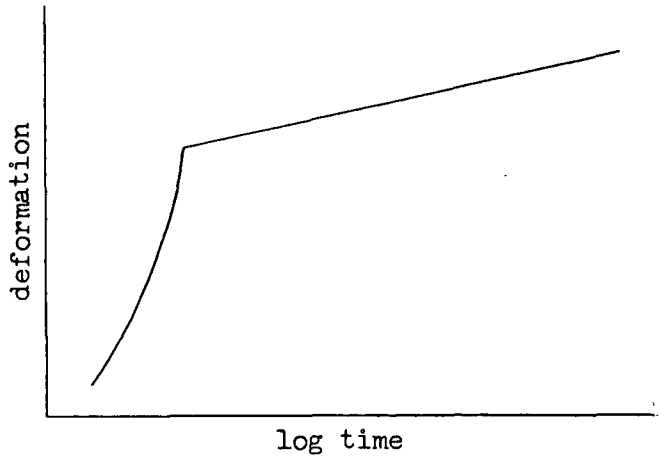

The initial high-rate deformation, however, is of particular interest in the present discussion. Wilder concluded that the response of deformation in this period is controlled by the flow of water. The acceleration of the system (mat and piston) is a result of two opposing actions, the driving force (compressive load) and the frictional force (resistance to flow). If the acceleration is small, the system may be considered to be in successive states of pseudoequilibrium, and the response of fibers to compression assumed to be almost instantaneous and without appreciable irreversible effects such as fiber slippage. This assumption awaits experimental verification.

3. Disturbances

When the acceleration is large (thin mats and high loads) the system may execute damped vibration, as actually observed by Wilder. In this case whether the compression behavior of fiber mats remains unchanged is not known. Moreover, cyclic disturbances may be imparted to the system by external causes (forced vibrations) which are common in laboratories and unavoidable on paper machines. A study of such effects will be pertinent to this project.

DYNAMIC DRAINAGE TESTER

The dynamic drainage tester was given by the hydrodynamics laboratory of Kimberly-Clark Corporation. It consisted of a tube and piston with the attached driving mechanism. For safety precaution the original glass tube was replaced by a Lucite tube. Continuous measuring instruments were added to the tester. The complete set-up is shown in Fig. 2. The details of the apparatus are described below.

DESCRIPTION OF THE TESTER

The Lucite forming tube is 7.6 cm. in diameter and 100 cm. tall. The top of the tube is fitted with two flanges between which a wire screen is clamped. The open end is covered in a box for the flow to return through a pipe by gravity into a receiver. The steel piston is fitted with a Teflon sleeve as a contact surface inside the tube to improve lubrication and sealing. The piston is rigidly connected with a rod or rack which is geared to a pinion. The number of teeth engaged in a single stroke is 59. The pinion is driven by a motor through a variable speed reducer engaged by a hand-operated clutch. The linear speed of the piston may be set from 1 to 100 cm. per sec.

Near the flanges on the tube wall is located a pressure tap which is connected by a plastic tubing to either of two transducers, covering a pressure range up to 700 cm. of water. The output of either transducer is received by an oscilloscope. The pressure trace on the oscilloscope is recorded by a Polaroid camera. The pressure transducers were calibrated against a manometer.

The nonuniform motion of the piston, which is to be discussed presently, can be measured with the aid of an accelerometer secured to the piston rack.

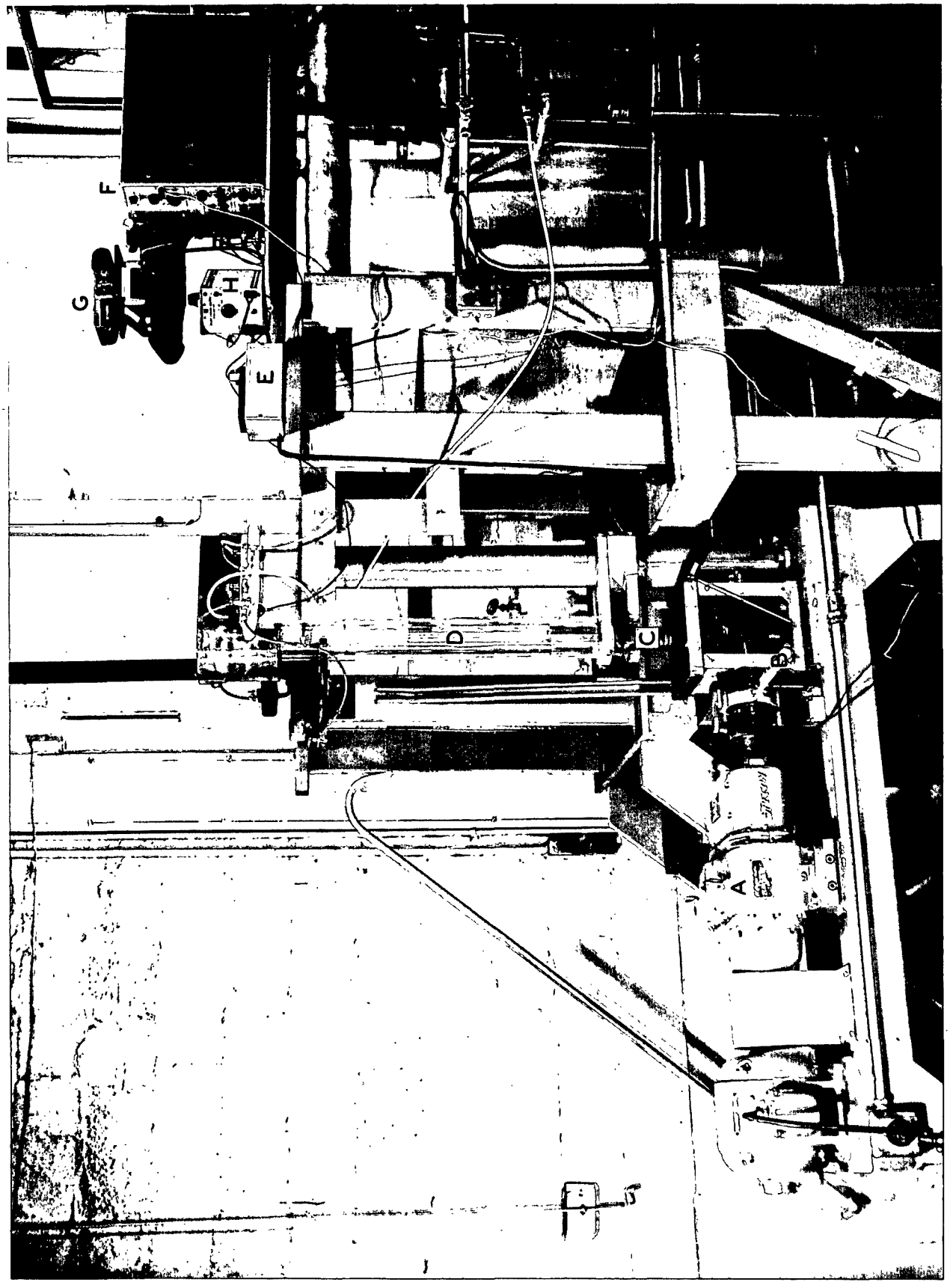

Figure 2. Dynamic Drainage Tester

A = Speed reducer, B = Clutch lever, C = Piston, D = Forming tube, E = Transducer power supply, F = Oscilloscope, G = Polaroid camera, H = Accelerometer signal amplifier

The signal from the accelerometer is transmitted through an amplifier to the oscilloscope from which an acceleration trace is recorded by the Polaroid camera. The characteristics and limitations of the pressure and acceleration measuring instruments are discussed in the Appendix.

PISTON MOTION

When the clutch is engaged, the inertial system including the piston rack, pinion, and the driven member of the clutch undergoes rapid acceleration to reach the driving speed. This initial acceleration is nonuniform as shown by the acceleration traces of Fig. 3. It is seen that the piston acceleration rises to a positive maximum, then falls to a negative minimum, and finally oscillates about the zero value. The indication of large deceleration is disturbing. After analysis of the instrument characteristics (see Appendix I) we concluded that the deceleration was probably due to the improper operation of the accelerometer. On this ground the initial part of the acceleration trace may be shifted upward to yield all positive values. The area under the reconstructed curve from the start of the motion to the zero value should be the driving speed. This was found to be very closely the case, as shown in Fig. 4, based on the data of Fig. 3.

The velocity curve is of the S shape. The initial acceleration time determined from a number of runs is well within 0.05 sec., most probably as low as 0.03 sec.

As previously discussed, the acceleration of the piston is proportional to the difference between the driving force of the motor and the resisting force of the driven system due to friction. At the instant the clutch is engaged, the motor drops to a slightly lower speed, and, as a result, develops more torque by

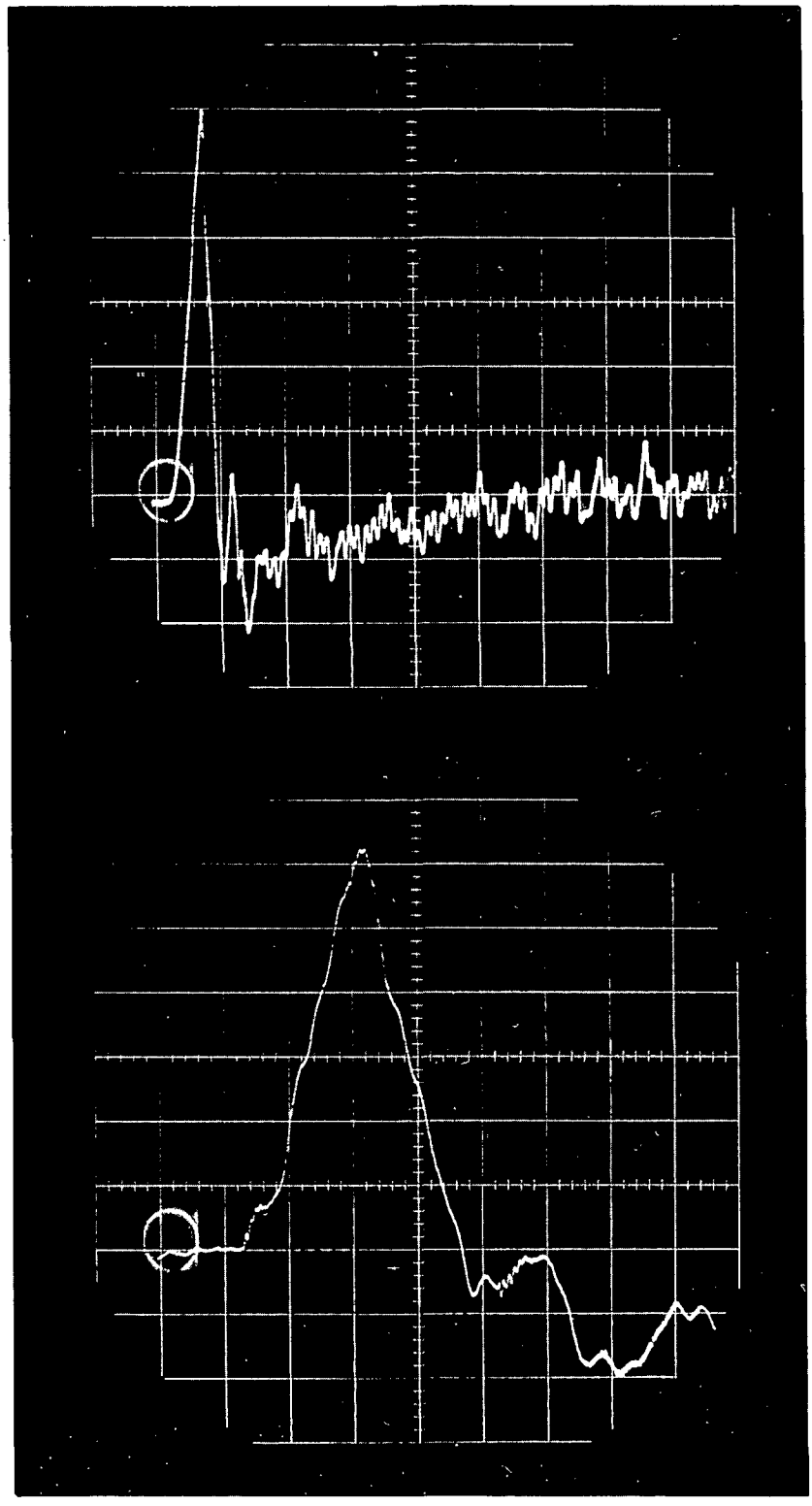

Figure 3. Initial Acceleration of Piston

Upper Exposure	Lower Exposure
Horizontal scale: 0.05 sec./div.	0.01 sec./div.
Vertical scale: arbitrary units	same

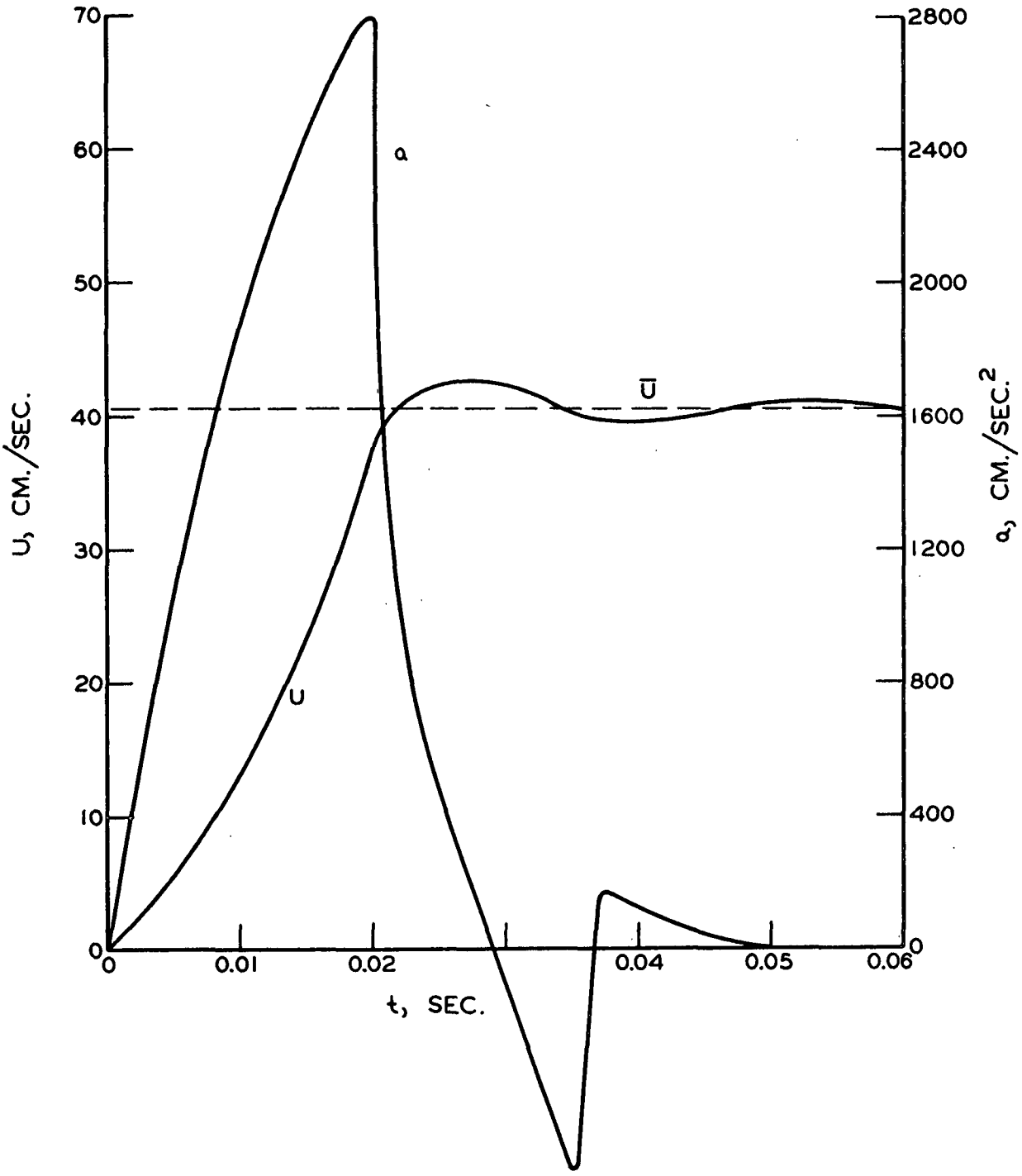

Figure 4. Corrected Piston Acceleration and Velocity

drawing more electric current until a constant value is reached. Meanwhile, the motion of the piston causes the friction to increase until a steady speed is attained. A force diagram may be depicted crudely in the following sketch:

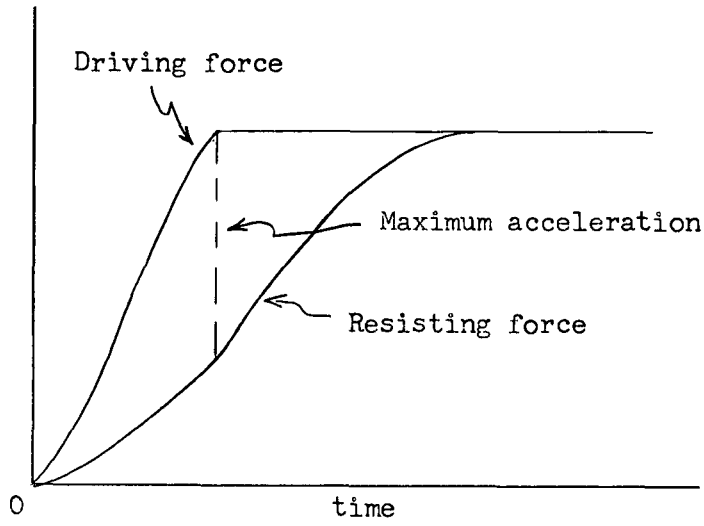

After an apparently steady speed is reached, the piston continues to exhibit oscillating acceleration and deceleration about the zero value, as revealed by the traces in Fig. 5. The oscillation is believed to be due to the nonuniform transmission of force in the gear engagement of the pinion and rack. The number of cycles in a stroke was found to coincide with the number of gear teeth engaged during a run. The frequency of oscillation, f, is therefore $59/t_s$, t_s being the elapsed time of a single stroke.

PRESSURE OSCILLATION

Because of the periodic acceleration, the piston velocity must also fluctuate about a mean value which is the piston travel divided by the stroke time. The fluctuating velocities imparted by the piston to the fluid in the tube causes similar fluctuations in the fluid pressure, as shown by Fig. 5.

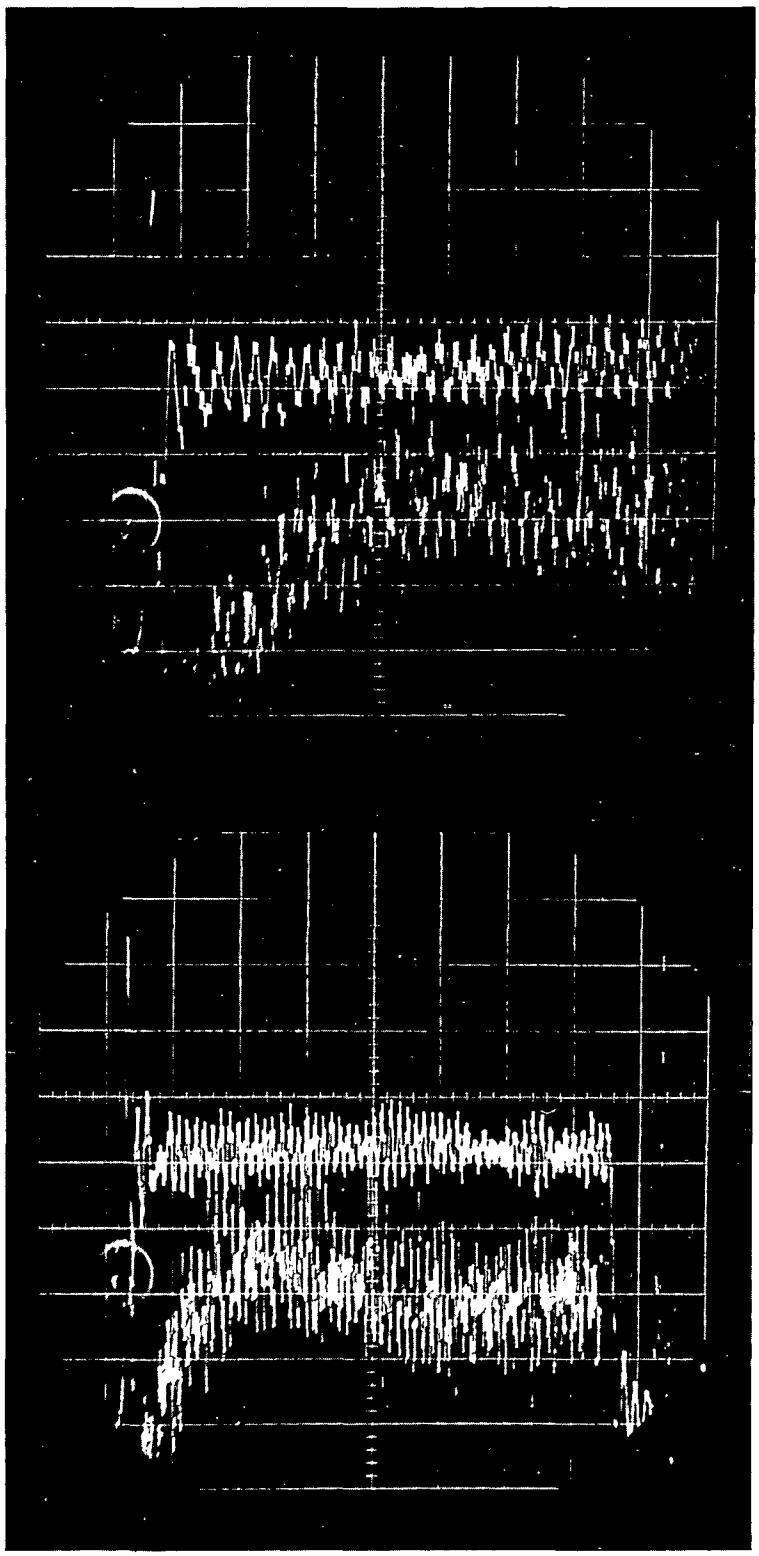

Figure 5. Pressure and Acceleration Traces (in Each Exposure the Upper Trace Is Pressure)

	Upper Exposure	Lower Exposure
Horizontal scale:	0.1 sec./div.	0.2 sec./div.
Vertical pressure scale:	100 cm. of water /div.	same
Mean pressure =	440 cm. of water	430 cm. of water

The pressure trace was obtained by inserting an orifice plate in the flanges as a flow restriction in order to attain a measurable pressure of water in the tube.

If the piston is thought to be in a simple harmonic motion, then its velocity and acceleration may be represented by the following equations:

$$U = \bar{U} + U_m \sin 2\pi ft \tag{6}$$

and

$$a = 2\pi f U_m \cos 2\pi ft \tag{7}$$

where U, $\bar{U}$, and U_m are the instantaneous, mean, and maximum velocities, respectively, a is the acceleration, f the frequency of oscillation, and t the elapsed time, referred to the origin when the mean velocity is first reached. It is to be noted that the peak value of acceleration is $2\pi f$ times the peak value of velocity, and they are 90° out of phase.

The pressure drop across the orifice is related to the flow velocity by the simplified orifice equation

$$\bar{U} = \frac{C}{\sqrt{\frac{A}{A_o} - 1}} \sqrt{\frac{2\overline{\Delta P}}{\rho}} = K\sqrt{\overline{\Delta H}} \tag{8}$$

where $\overline{\Delta H}$ or $\overline{\Delta P}/\rho g$ is the time-mean fluid head across the orifice, A and A_o are the cross-sectional areas of the tube and orifice, respectively, and C is the orifice coefficient. The pressure transducer measures the pressure in the tube against atmospheric pressure which is also the downstream pressure of the orifice. The orifice coefficient, C, calculated from the measured values of $\bar{U}$ and $\overline{\Delta H}$ was found to be in agreement with the known value, 0.6, for

highly turbulent flow through a sharp-edged orifice. The major frequency of pressure oscillation was found to be the same as that of acceleration. On this basis we assume that Equation (8) also applies to any instant of flow. The instantaneous head may be expressed by

$$\Delta H = \frac{1}{K^2} (\bar{U} + U_m \sin 2\pi ft)^2 \qquad (9).$$

Thus, the values of U_m may be derived from the independent measurements of acceleration and pressure. They are summarized in Table I.

TABLE I

PEAK VALUES OF VELOCITY

$\bar{U}$, cm./sec.	$\overline{\Delta H}$, cm. H_2O	C	U_m, Eq. (9), cm./sec.	U_m, Eq. (7), cm./sec.
23.2	94	0.56	2.7	0.76
27.6	132	0.56	1.8	0.59
30.8	160	0.57	1.7	0.56
39.4	210	0.63	3.2	0.69
51.3	440	0.57	2.4	0.80

It is seen that the values of U_m derived from the pressure measurement are larger than those from the acceleration measurement by a factor of three. We believe that the latter is more reasonable because the peak values of pressure over the mean, $(2\bar{U}U_m + U_m^2)/K^2$, are amplified by resonance of the pressure transducer due to external disturbances. This point is discussed in Appendix II.

From Fig. 5 it is also seen that the pressure reaches its mean value before the lapse of 0.05 sec. Then, in accordance with the orifice equation (8)

the mean piston or water velocity is also attained within this time, in agreement with the previous conclusion concerning the initial motion of the piston.

In summary, the piston accelerates from zero to a mean velocity within 0.05 sec. It continues to oscillate about the mean velocity with a major frequency of $59/t_s$ and an amplitude less than one cm./sec. The pressure of water in the tube also oscillates about a mean value with the same major frequency and an exaggerated amplitude due to external disturbances. The time-mean values of velocity and pressure, however, are reliable.

SHEET-FORMING TESTS

For preliminary purposes 3-denier dacron fibers were chosen. They have the following characteristics:

Fiber diameter, d_f		1.71×10^{-3} cm.
Fiber length, L_f		0.53 cm.
Specific surface, S_v		2,340 sq. cm./cc.
Specific volume, v		0.709 cc./g.
Compressibility constants,	M	0.0066 c.g.s. units
and	N	0.254

The wire screen used was a conventional 52 by 52-mesh wire. On the basis of Estridge's work (6), the initial retention of the particular fibers on this screen was estimated to be practically complete in the absence of disturbances. The pressure drop-flow rate data for the screen alone are shown in Fig. 6.

The fibers were dispersed in an overhead feed tank at a low consistency, using the regular laboratory procedure. The tube of the dynamic drainage tester was rapidly filled with the fiber suspension by gravity from the piston upward. As soon as the suspension reached the screen, the clutch was engaged and at the same time microswitches were closed to activate an electric timer and the recording instrument. The piston motion was arrested by a mechanical clutch release when the piston reached the limit of its travel. The run time was of the order of one second. After the run the fibers in the tube were collected and weighed.

REPRODUCIBILITY

To test the reproducibility of data a series of nine runs were made at the same piston velocity. For each run the time-mean pressure drops were

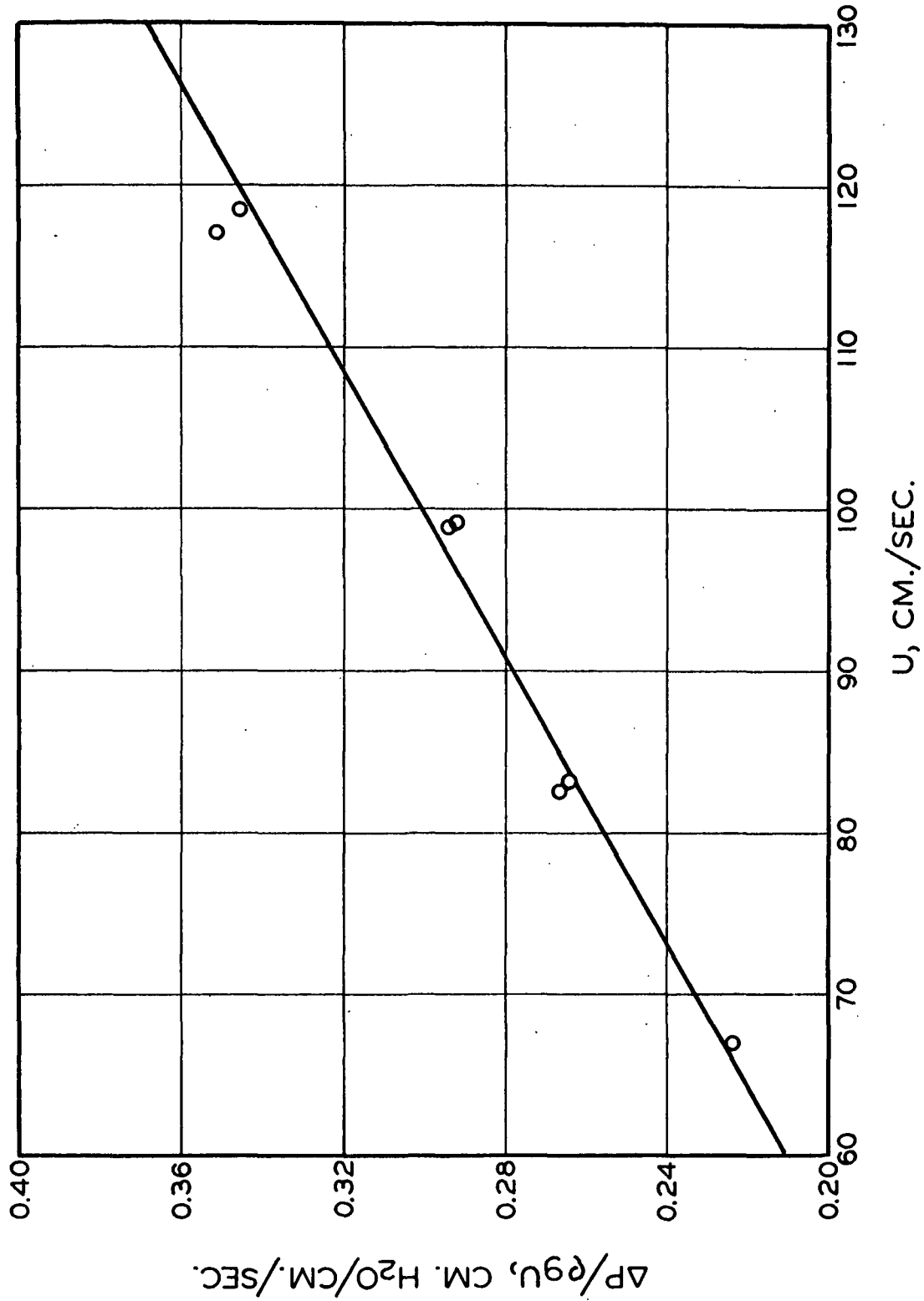

Figure 6. Calibration of the Wire Screen

translated from the pressure trace at arbitrary intervals. The corresponding basis weights were determined by

$$\frac{W}{A} = s\rho\bar{U}(t - t_o) \qquad (10)$$

where s is the consistency of the fiber suspension, ρ the density of suspension, and $t - t_o$ the corrected time. The time correction arises from the difficulty in synchronizing the initiation of drainage and pressure trace. The pressure trace is extrapolated to zero pressure which yields the necessary correction, t_o. The experimental results of the nine runs are summarized in Table II. Sample calculations are given in Appendix III.

TABLE II

REPRODUCIBILITY OF TEST RESULTS

$\bar{U}$ = 100 cm./sec.; $\mu = 9.25 \times 10^{-3}$ poise

$\bar{\Delta P} \times 10^{-3}$, dynes/sq. cm.	51	90	129	168	208	245	286	325
$s \times 10^4$, g./g.	$W/A \times 10^4$, g./sq. cm.							
4.93	40	78	122	157	200	236	272	311
4.48	41	89	126	166	202	238	276	308
4.40	49	92	134	172	208	243	280	316
4.58	49	96	138	175	211	248	286	322
4.57	50	91	130	166	208	240	274	304
4.63	51	98	135	171	210	251	288	330
4.35	54	93	134	170	205	241	277	311
4.63	56	98	139	179	213	249	286	321
4.08	60	101	138	179	216	250	287	--
Max. discrepancy	1.5	1.28	1.14	1.14	1.08	1.06	1.06	1.06
Av. of 9 runs	50	93	133	171	208	244	281	316
Calcd. from Eq. (1)	50	89	125	163	201	237	271	307
Deviation	1.0	1.04	1.06	1.05	1.04	1.03	1.04	1.03

In Table II the maximum discrepancies among the runs are shown by the ratio of the two extreme values. It is seen that the discrepancies are very large (50%) at early times and gradually narrow down to 6% toward the end of the run.

This trend of discrepancy is largely attributable to the translation of pressure drops and corresponding time from the pressure trace. First, it is more difficult to read the mean pressure at early times because of the large pressure oscillations (see the pressure trace shown with the sample calculations in the Appendix). Second, the percentages of error involved in reading small pressures are larger. Third, the pressure readings must be corrected for the screen resistance to yield the pressure drop across the mat. This correction by difference results in errors when the pressure readings are small. The error of pressure measurement and translation is about 5 cm. of water, and the error in screen calibration is about 1 cm. H_2O. Fourth, the uncertainty involved in the correction of time is about 0.005 sec. This time correction is again by difference. In addition, the consistency measurement from a fiber mass of about 2 g. involves an error of 0.01 g. The mean velocity can be determined within 1 cm. per sec. Thus, the combined maximum error would account for $\pm$18% in basis weight at the lowest pressure (50 cm. H_2O) and $\pm$2% at the highest pressure (300 cm. H_2O).

If these errors occurred randomly with a normal distribution, then the medians of the runs would be in close agreement with the average values. This appears to be the case.

AGREEMENT WITH THE CORRELATION

Having established the credibility of the average values of data, we proceed to make a comparison with the correlation. The values of basis weight calculated from Equation (1) at the corresponding pressure drops are listed below the average experimental values. The agreement is surprisingly good, the largest deviation being only 6% which is well within the precision of the correlation.

More runs were made at different velocities. The results are shown in Fig. 7. The circles are data of duplicate runs and the solid curve represents the correlation. The maximum deviation is within 10%.

The apparent absence of nonequilibrium effects in these experiments may be attributed to three factors: (1) low compressibility of dacron fibers, (2) dilute suspensions, and (3) insufficiently short forming times.

The response of viscoelastic fibers to compression may be divided into two parts. The elastic response is assumed to be instantaneous and the viscous response to be time dependent. The dacron fibers used have low compressibility. This is reflected in Fig. 7 by the nearly linear relationship between the pressure drop and basis weight or mat thickness. For such fibers the time-dependent effects are small and difficult to detect. Flow pulsations and pressure fluctuations in the tester were probably not of sufficient magnitude to cause a change in the compressibility of dacron fibers.

When a sheet is formed from a dilute suspension, the motion of fibers, once deposited, is negligible. In the absence of appreciable motion the fibers

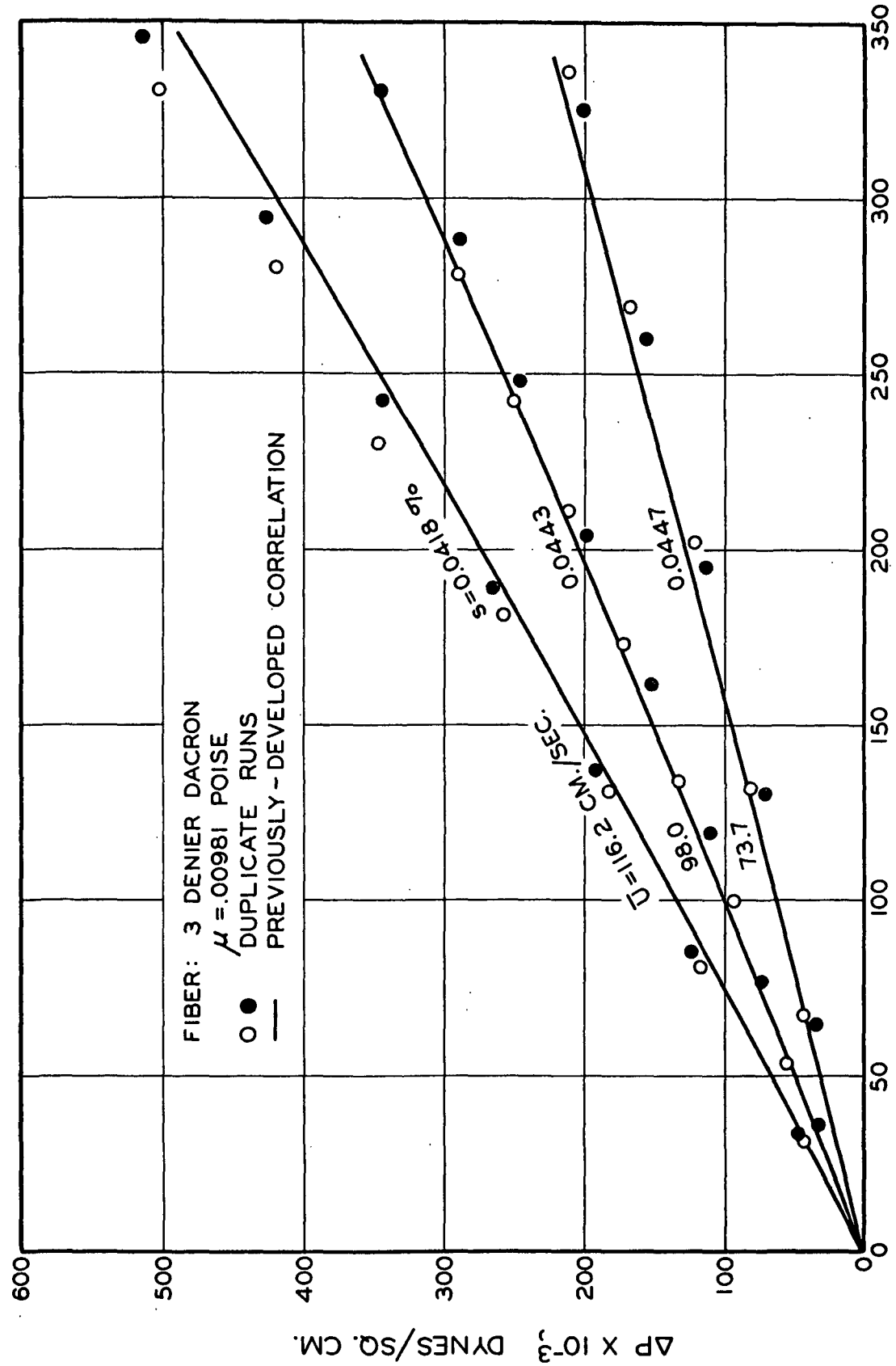

Figure 7. Comparison of Drainage Data with the Correlation

are in a state of equilibrium or at least quasi-equilibrium. Their behavior under fluid stresses would remain the same as in slow filtrations.

The time scale from slow filtrations to rapid drainage in the dynamic tester is only two decades. This reduction may not be sufficient to show the time-dependent effects. Furthermore, the compressibility of fibers might be dependent on the rate of pressure rise. On a fourdrinier both the time scale and the rate of pressure rise are about another two or three decades away from the present testing conditions, as shown in the following estimate:

	Slow Filtration	Drainage Tester	Table Roll
Forming time, sec.	10	10^{-1}	10^{-3}
Rate of pressure rise, dynes/(sq. cm.)(sec.)	10^{3}	10^{6}	10^{9}

The apparent agreement of the present results with the previous correlation leads to the conclusion that for relatively incompressible fibers in dilute suspensions the drainage behavior and sheet structure remain unchanged so long as the flow is stable.

CONTINUING WORK

From the foregoing discussion it appears that the future investigations should be conducted in three successive phases: (1) using wood pulps to ascertain the compressibility effects, (2) changing to high consistencies for acceleration effects, and (3) further shortening the forming time and increasing the rate of pressure rise.

With the present tester only the first phase of investigating wood pulps in dilute suspensions is feasible. To minimize the complication of fines a classified pulp will be used. Refining of the pulp will be very light to

avoid excessive pressure drops. The results of the tests will be again compared with those from slow filtrations under nearly equilibrium conditions.

The second and third phases of investigation will necessitate drastic modifications of the apparatus or most likely a new design.

NOMENCLATURE

A = area, sq. cm.; an integration constant

a = acceleration, cm./sq. sec.

B = amplification factor

b' = inertial resistance coefficient

C = orifice coefficient; capacitance, $\mu\mu f$

d_f = fiber diameter, cm.

e = voltage, millivolts

F = force, dynes

f = frequency, 1/sec.

f' = friction factor

g = gravitational constant, cm./sq..sec.

H = fluid head, cm. H_2O

i = current, milliamp.

K = constants

k = Kozeny factor; constants

k_o = a constant

L_f = fiber length, cm.

M = compressibility coefficient, c.g.s. units

m = mass, g.

N = power of compressibility function

P = pressure, dynes/sq. cm.

R = resistance, meg Ω

Re' = Reynolds number

S_v = specific surface, sq. cm./cc.

s = consistency, g./g.

$\underline{t}$ = time, sec.

$\underline{U}$ = velocity, cm./sec.

$\underline{v}$ = specific volume, cc./g.

$\underline{W}$ = mass of fibers, g.

α = a constant

β = a constant

ϵ = porosity

θ = angle, rad.

μ = viscosity, poises

ρ = density, g./cc.

σ = angular frequency, rad./sec.

ϕ = angle, rad.

ψ = angle, rad.

ω = angular frequency, rad./sec.

LITERATURE CITED

1. Ingmanson, W. L., Tappi 42, no. 6:449(1959).

2. Wrist, P. E., Pulp Paper Mag. Can. 55, no. 6:115(1954).

3. Taylor, G. I., Pulp Paper Mag. Can 57, no. 3:267(1956).

4. Progress Report in preparation, Project 2210, The Institute of Paper Chemistry.

5. Wilder, H. D. The compression creep properties of wet pulp mats. Doctor's Dissertation. Appleton, Wis., The Institute of Paper Chemistry, 1960.

6. Estridge, R. The initial retention of fibers by wire grids. Doctor's Dissertation. Appleton, Wis., The Institute of Paper Chemistry, 1962.

THE INSTITUTE OF PAPER CHEMISTRY

S. T. Han

S. T. Han

L. R. White

L. R. White

Engineering and Technology Section

APPENDIX I

ACCELERATION MEASUREMENT

A Model 2217 Endevco Accelerometer was used to measure piston acceleration. Its sensing element is a piezoelectric crystal which does not require a power supply. A schematic diagram of the circuit is shown below:

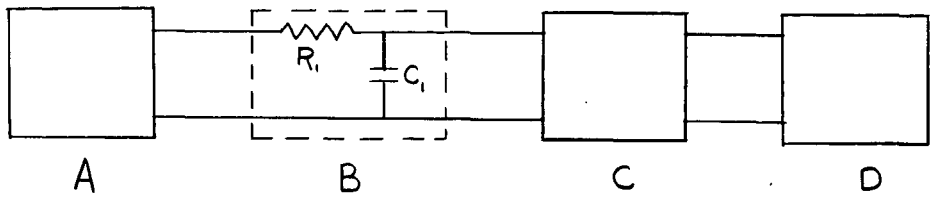

A - Model 2217 Endevco Accelerometer

B - Filter, R_1 = 40 megΩ; C_1 = 240 $\mu\mu$f

C - Keithley Model 102B decade isolation amplifier

D - Tektronix Type 502 dual-beam oscilloscope

Because of the high vibration level of the equipment it was necessary to filter the accelerometer output in order to observe the accelerations due to nonuniform engagement of the rack and pinion of the tester. The influence of the filter on input signals may be found from analysis of the following circuit:

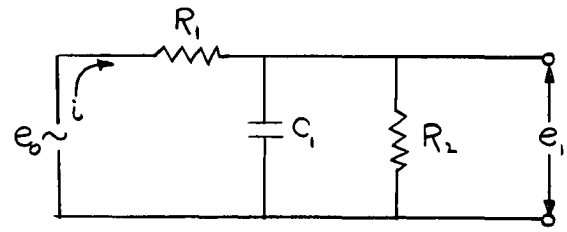

where R_1 is the filter resistor, R_2 is the input circuit resistance of the amplifier, and C_1 is the filter capacitor. In general,

$$i = \frac{e_o - e_1}{R_1} = C_1 \frac{de_1}{dt} + \frac{e_1}{R_2}$$

or

$$e_o = R_1 C_1 \frac{de_1}{dt} + (1 + \frac{R_1}{R_2})e_1 \qquad (11),$$

where $\underline{i}$ is current, and $\underline{e_o}$ and $\underline{e_1}$ are input and output voltages. It will be noted that $\underline{e_1}$ is the observed signal while $\underline{e_o}$ is the signal which is proportional to acceleration, i.e.,

$$a = k_o e_o \qquad (12),$$

where $\underline{k_o}$ is the proportionality constant relating voltage and acceleration.

INITIAL ACCELERATION

The time required to accelerate the piston to its steady driving speed must be short, and study of the early portions of a number of acceleration traces has been made in order to determine the time required to accelerate the piston.

Figure 3 in the text shows the filtered accelerometer signal $(\underline{e_1})$ for the early part of a run. Examination of the upper trace shows that the initial sharp spike is followed by a gradual deceleration. Consideration of the characteristics of the driving mechanism led to suspicion that the indicated deceleration was fictitious and the result of instrument error. It was also found that deceleration or negative undershoot after a sudden acceleration is

encountered frequently in the study of shock pulses and is caused by charge leakage off the accelerometer.

Because of this problem, observed acceleration data must be modified in order to obtain accurate values of acceleration and velocity. Piston velocity as a function of time may be obtained by integrating Equation (11):

$$U = k_o \int_{t=0}^{t=t} e_o dt = k_o[R_1 C_1 e_1(t) + (1 + \frac{R_1}{R_2}) \int_{t=0}^{t=t} e_1 dt] \quad (13).$$

Computation of velocity provides a check on the validity of acceleration data because the velocity computed from Equation (12) should be very near the average value after the period of initial acceleration has elapsed. The acceleration trace of Fig. 3 was modified to yield the corrected acceleration and velocity by means of Equations (12) and (13). The results have been shown in Fig. 4. Similar computations were performed on a total of seven traces, and in five out of seven the agreement between the calculated and measured velocities was very good. In addition, it was shown that the initial acceleration time was less than 0.03 second in each case.

The details of the computation for Fig. 4 are given as follows. Three equations were used to describe the corrected acceleration trace.

$$e_1 = 4120t \qquad 0 < t < 0.02$$

$$e_1 = 82.4 - 4650(t - 0.02) \qquad 0.02 < t < 0.035$$

$$e_1 = 12.7 - 520(t - 0.035) \qquad 0.035 < t < 0.0594$$

where t is in seconds and e_1 is in mv. The following values were used for the circuit constants:

$$R_1 = 40 \times 10^6 \Omega$$

$$R_2 = 400 \times 10^6 \Omega$$

$$C_1 = 240 \times 10^{-12} f$$

$$k_o = 22.1 \frac{\text{cm./sec.}^2}{\text{mv.}} .$$

When these values are substituted into Equations (11), (12), and (13), we obtain

$$a = k_o e_o = 22.1[(0.96 \times 10^{-2})\frac{de_1}{dt} + 1.1e_1]$$

$$U = k_o \int_{t=0}^{t=t} e_o dt = 22.1[(0.96 \times 10^{-2})e_1(t) + 1.1 \int_{t=0}^{t=t} e_1 dt .$$

Values of $\underline{a}$ and $\underline{U}$ were thus computed as functions of time.

OSCILLATORY ACCELERATION

During any run the velocity of the piston of the drainage tester fluctuates about its mean value. The magnitude of these velocity fluctuations has been computed from acceleration and pressure data, and the details of this computation are given as follows.

First of all, the influence of the filter will be found on oscillating input signals. For the purpose of the discussion of oscillating piston velocity, a sinusoidal variation has been assumed. This is not strictly correct because (1) more than one frequency is present and (2) although the curve is periodic, it is not simply harmonic. However, the labor required to carry out a more detailed analysis is not justified for this aspect.

The circuit is the same as previously shown. As before,

$$i = \frac{e_o - e_i}{R_1} = C_1 \frac{de_i}{dt} + \frac{e_i}{R_2} \qquad (11).$$

Assuming

$$e_o = e_m \sin\omega t \qquad (14),$$

where $\omega = 2\pi f$ and e_m is the amplitude, then

$$\frac{de_i}{dt} + \left(\frac{1}{R_1 C_1} + \frac{1}{R_2 C_1}\right) e_i = \frac{e_m}{R_1 C_1} \sin\omega t \qquad (15),$$

which is a first-order linear differential equation, and may be solved readily to give

$$e_i = \frac{e_m}{R_1 C_1} \frac{(k_1 \sin\omega t - \omega\cos\omega t)}{k_1^2 + \omega^2} - \frac{\omega e_m}{R_1 C_1 (k_1^2 + \omega^2)} e^{-k_1 t} \qquad (16),$$

where

$$k_1 = \frac{1}{C_1}\left(\frac{1}{R_1} + \frac{1}{R_2}\right) \qquad (17).$$

Ignoring the transient, it may be shown that

$$\frac{e_i}{e_o} = \frac{1}{\sqrt{\left(1 + \frac{R_1}{R_2}\right)^2 + (R_1 C_1 \omega)^2}} \qquad (18),$$

and e_i will lag e_o by the angle

$$\varphi = -\arctan\frac{\omega}{k_1} = -\arctan\frac{\omega C_1 R_1}{1 + \frac{R_1}{R_2}} \qquad (19).$$

Using Equation (18), the attenuation ratio introduced by the filter may be computed. It will be noted that the attenuation ratio is dependent on ω or the frequency of the signal. Figure 8 shows $\underline{e_1}/\underline{e_o}$ as a function of $\underline{f}$, using the following values:

$$R_1 = 40 \text{ meg}\Omega$$

$$C_1 = 240 \ \mu\mu f$$

$$R_2 = 400 \text{ meg}\Omega$$

The figure indicates the function of the filter; input signals of high frequency are strongly attenuated, permitting examination of lower frequency components of the signal.

The computation of $\underline{U_m}$ will be illustrated with Fig. 5. It has been shown that

$$U_m = \frac{a}{2\pi f \cos(2\pi ft)} \qquad (7).$$

$\underline{U_m}$ may therefore be conveniently computed by reading from the acceleration trace an average zero-to-peak acceleration at $\cos 2\pi ft = 1$.

For the run illustrated,

$$a \cong 3.3 \text{ mv.} \left(22.1 \frac{\text{cm./sec.}^2}{\text{mv.}}\right) = 73 \text{ cm./sec.}^2$$

$$f = \frac{59}{1.50} = 39.3 \text{ c.p.s.}$$

$$U_m = \frac{73}{6.28(39.3)} = 0.30 \text{ cm./sec.}$$

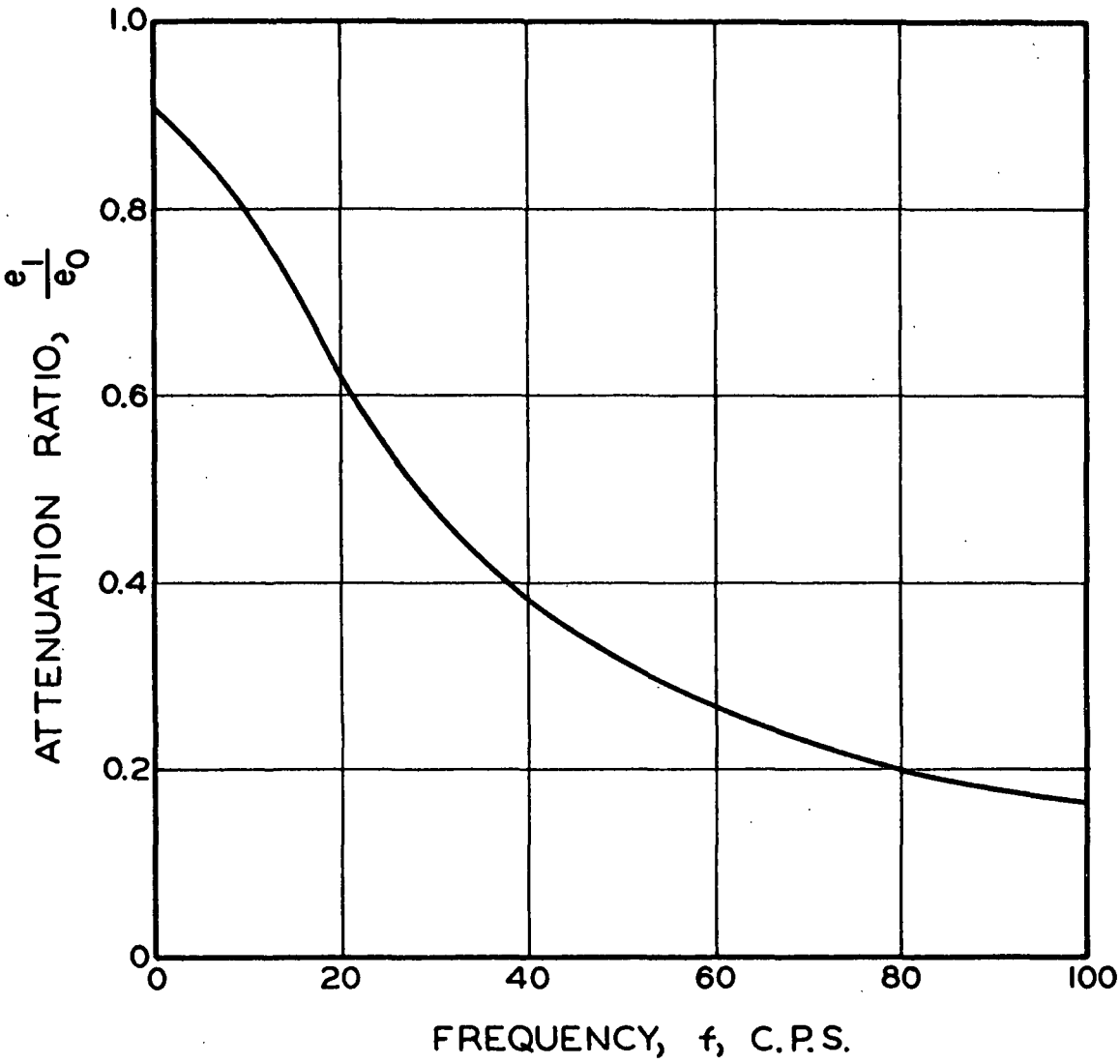

Figure 8. Signal Attenuation

This value must be corrected for filter attenuation, $\underline{e}_1/\underline{e}_o$, determined at $\underline{f}$ = 39 c.p.s. from Fig. 8 as follows:

$$\frac{e_1}{e_o} = 0.38$$

$$U_m = \frac{0.30}{0.38} = 0.80 \text{ cm./sec.}$$

A value of $\underline{U}_m$ may also be computed from the pressure trace of Fig. 5, using the previously developed Equation (9) for $\Delta\underline{H}_m$ at $\sin(2\pi \underline{f}t) = 1$:

$$U_m = \sqrt{\bar{U}^2 + K^2 \Delta H_m} - \bar{U} \qquad (20),$$

where $\Delta\underline{H}_m$ is the average value of maximum pressure fluctuation minus the mean pressure drop across the orifice. For the particular run,

$$\Delta\underline{H}_m = 40 \text{ cm. of water,}$$
$$\underline{\bar{U}} = 51 \text{ cm./sec., and}$$
$$\underline{K} = 2.57.$$

Using these values,

$$U_m = \sqrt{(51)^2 + (2.57)^2(40)} - 51 = 2.4 \text{ cm./sec.}$$

The most reasonable explanation for the discrepancy between this result and the value computed from acceleration data is that resonance of the pressure transducer amplifies the pressure fluctuation. This problem is discussed in Appendix II.

APPENDIX II

PRESSURE MEASUREMENT

Two Statham pressure transducers (Models PM 131 TC ±2.5-350 and PG TC-10-350) were used; one measures pressures over the range 0 to 175 cm. of water and the other measures pressures over the range 0 to 700 cm. of water. The power supply for either transducer is shown schematically below.

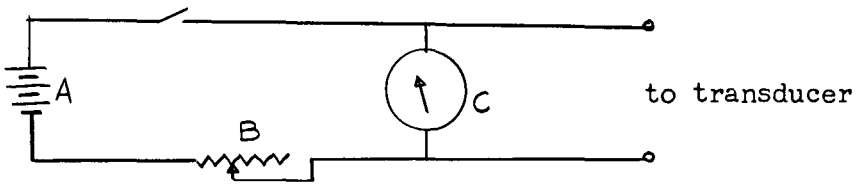

A - 6-volt battery

B - 10-turn Beckman Helipot

C - 0-10 v., d.c. voltmeter

The same oscilloscope was used to receive the pressure signals. Ordinary potentiometric-type recorders are much too slow and oscillographs are not sufficiently versatile for the present purpose.

Depending on the pressure range, either a water or mercury manometer was used to calibrate the pressure transducer. Calibration is accomplished simply by applying a steady pressure to the transducer and observing the trace on the oscilloscope. This procedure eliminates individual errors in oscilloscope, power supply, and transducer sensitivities; adjustment of the power supply voltage permits selection of a convenient over-all sensitivity.

RESONANCE

Figure 9 shows the output of the pressure transducer when the line leading to the transducer is plugged and rapped gently. The damped oscillatory signal is evidently due to resonance of the transducer.

As a first approximation, the following differential equation will be used to describe the oscillation of the transducer itself.

$$m \frac{d^2x}{dt^2} + K_1 \frac{dx}{dt} + K_2 x = 0 \qquad (21).$$

This equation is simply a statement of Newton's second law of motion for oscillating particles, in which a retarding force proportional to the velocity is included. The quantity $\underline{m}$ represents the mass of the accelerated material, $\underline{K_1}$ represents the damping constant, which depends on the viscosity of the medium and other energy-dissipating agencies operating in the transducer, and $\underline{K_2}$ is the spring constant of the transducer. For the transducer in air, both $\underline{m}$ and $\underline{K_1}$ will be small, the mass of material being accelerated will be mostly that of the transducer itself, and the viscosity of the air will be small. The value of $\underline{K_1}$ in this case would be determined by the energy-dissipating agencies in the transducer. In water, however, both $\underline{m}$ and $\underline{K_1}$ will be large, and the ratio of $\underline{K_2}/\underline{m}$ will be small. The effect of the medium on the performance of the transducer can be shown by consideration of the solution of Equation (21).

Let $\underline{K_1}/\underline{m} = \alpha$ and $\underline{K_2}/\underline{m} = \beta$; then the solution of Equation (21) may be written as

$$x = Ae^{-(\alpha/2)t} \cos(\omega t + \phi) \qquad (22)$$

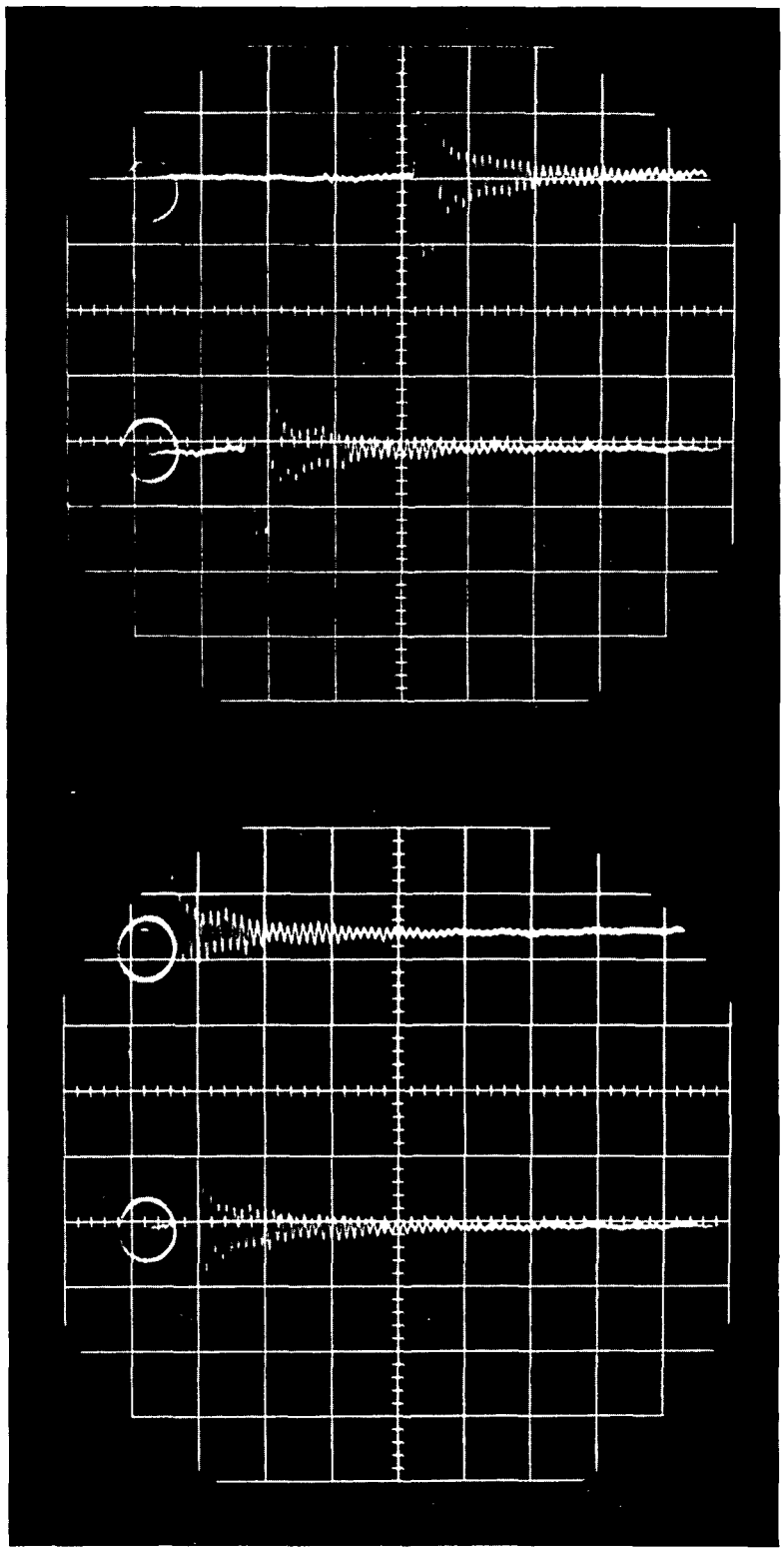

Figure 9. Resonance of Pressure Transducer

Horizontal scale: 0.05 sec./div.

where $\omega^2 = \beta^2 - (\alpha^2/4)$ and $\underline{A}$ and ϕ are arbitrary integration constants. If $\alpha = 0$ (no damping), the natural frequency of vibration is

$$\omega_o = \sqrt{\beta} \qquad (23);$$

with damping,

$$\omega_o = \sqrt{\beta - (\alpha^2/4)} \qquad (24).$$

Whenever a dense pressure medium is employed, β will be small since it is simply the ratio of $\underline{K_2}$, a constant for a given instrument, to $\underline{m}$, the mass of material being accelerated. Both the mass of the moving parts in the transducer and the pressure medium in the region of the diaphragm comprise $\underline{m}$ since the medium near the diaphragm must be accelerated by its motion. The natural frequency, ω_o, will be much lower for a transducer when it is used with water than with air. Figure 9 demonstrates this clearly. The natural frequency of the instrument specified by the manufacturer is 5000 c.p.s.; the observed frequency in water is only 170 c.p.s., a very substantial decrease. The significance of this result can be seen from the following discussion of forced vibration.

FORCED VIBRATION

The following equation describes the forced vibration of a spring:

$$\frac{d^2x}{dt^2} + \alpha \frac{dx}{dt} + \beta x = \frac{F}{m} \cos\sigma t \qquad (25),$$

where $\underline{F}$ is an external force and σ the angular frequency. Because the drainage tester generates oscillatory pressure waves, Equation (25) may be utilized to describe the qualitative behavior of the pressure transducer. The solution of Equation (25) is tabulated in the literature and may be rewritten in the present nomenclature:

$$x = Ae^{-(\alpha/2)t}\cos(\omega t + \theta) + \frac{(F/m)\cos(\sigma t + \phi)}{\sqrt{(\beta - \sigma^2)^2 + \alpha^2\sigma^2}} \quad (26);$$

$$\phi = -\arctan\frac{\alpha\sigma}{\beta - \sigma^2} \quad (27),$$

The term involving the exponential function and the arbitrary integration constants A and θ will vanish as t becomes large and is of no concern here.

The above equations permit determination of the amplitude and the phase shift of the imposed vibration. It will be noted that the frequency of the imposed vibration, $\sigma/2\pi$, is not altered, but a phase shift, ϕ, and an amplification factor, $B = 1/\sqrt{(\beta - \sigma^2)^2 + \alpha^2\sigma^2}$, must be considered.

Both ϕ and B depend only on σ since β and α are constant for a given system. Figures 10 and 11 show the variation of B and ϕ with σ, respectively. (Values of α and ω_o were computed from Fig. 9.) The important point to note is the effect of the natural frequency, ω_o, on ϕ and B. When the imposed frequency equals the natural frequency, B is a maximum and ϕ is -90°, i.e., the transducer output lags the applied signal by 90°. If ω_o were larger, ϕ would be negligible and B would be a constant over the frequency range of interest in connection with the drainage tester. Because B and ϕ are significant, it is not possible to determine accurately the phase and amplitude of oscillating pressure traces. Although the primary frequency is never greater than 100 c.p.s., vibrations in the neighborhood of ω_o always occur. These vibrations are transmitted through the water to the transducer, create resonance, and make it difficult to analyze the results quantitatively.

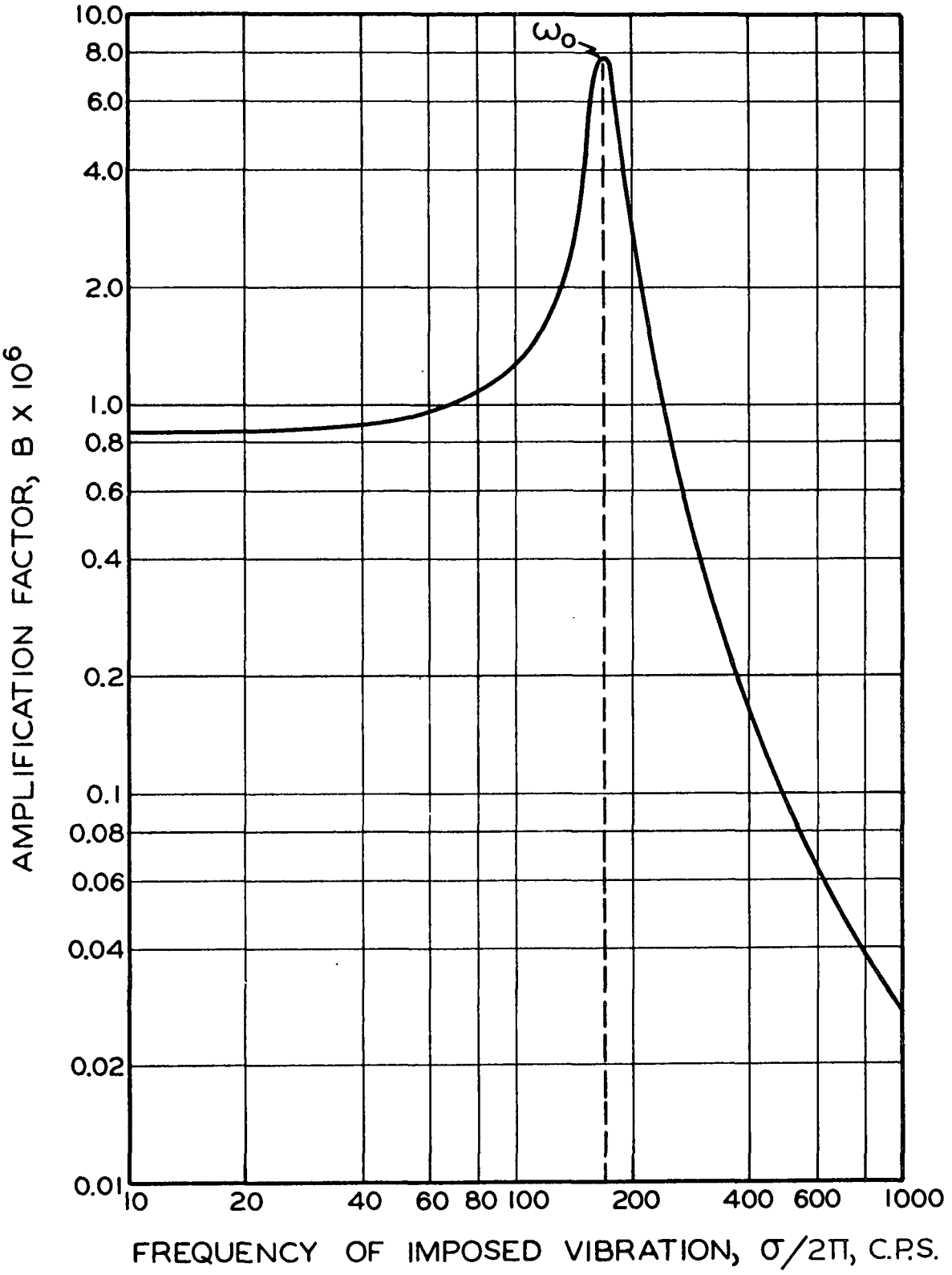

Figure 10. Amplification Factor of Pressure Transducer

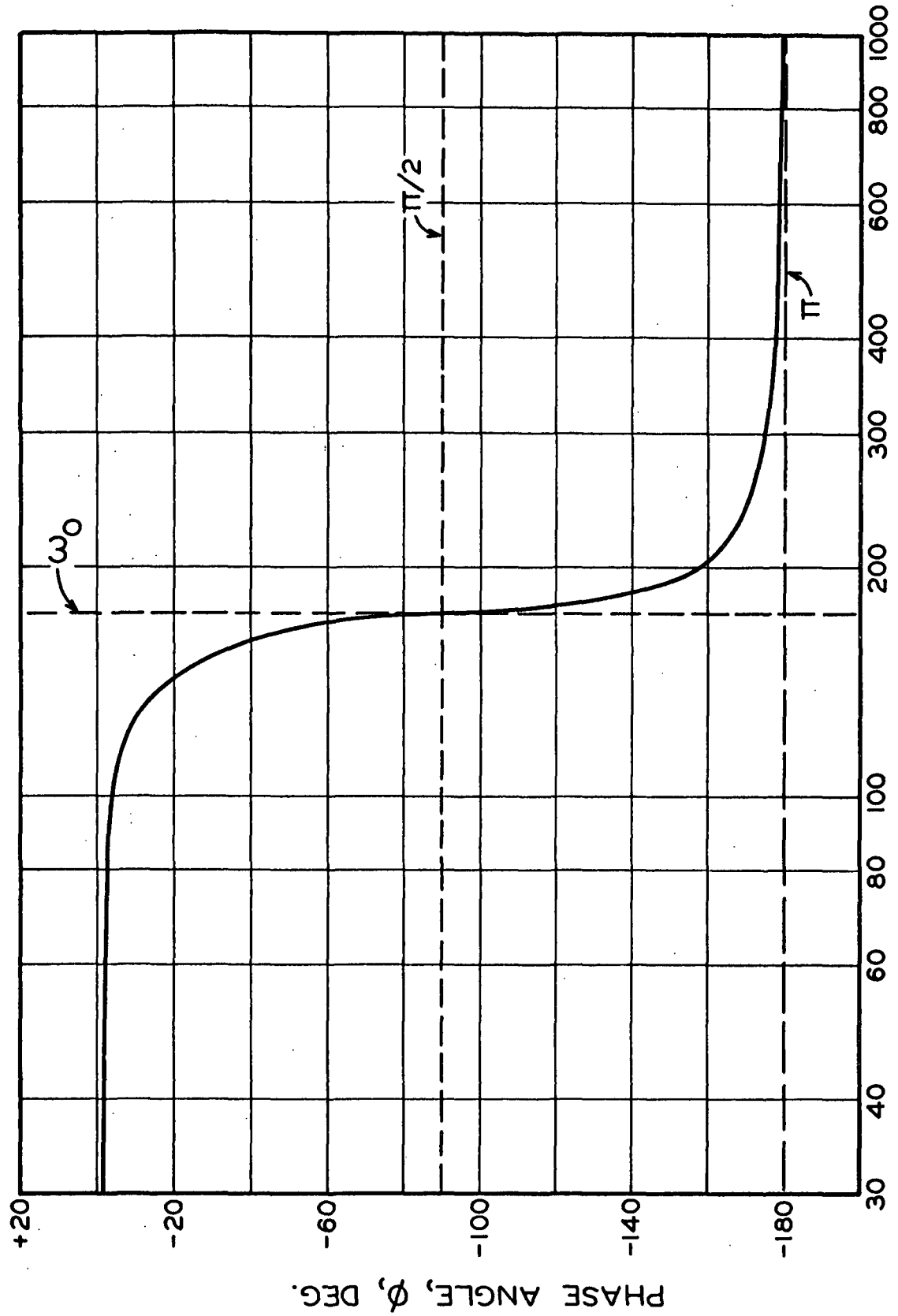

Figure 11. Phase Shift of Pressure Transducer

APPENDIX III

SAMPLE CALCULATIONS

The pressure drop-basis weight curve for a high-velocity filtration may be predicted from the following equations:

$$\frac{\Delta P}{W/A} = \left[\frac{\bar{k}(1-\bar{\epsilon})}{\bar{\epsilon}^3}\right] v S_v^2 \mu U + 0.1 \left[\frac{\bar{k}^{-1/2}}{\bar{\epsilon}^3}\right] v S_v \rho U^2 \qquad (1)$$

$$\bar{k} = \frac{3.5\bar{\epsilon}^3}{(1-\bar{\epsilon})^{1/2}} [1 + 57(1-\bar{\epsilon})^3] \qquad (2)$$

$$\bar{\epsilon} = 1 - (1 - \frac{N}{2}) v (M \Delta P^N) \qquad (3)$$

The curve of Fig. 7 was computed from the following values for 3-denier dacron fibers:

$\underline{v}$ = 0.709 cc./g.

$\underline{S_v}$ = 2340 sq. cm./cc.

$\underline{M}$ = 0.0066 c.g.s. units

$\underline{N}$ = 0.254 c.g.s. units

$\underline{A}$ = 45.6 sq. cm.

μ = 0.00981 poise

$\underline{U}$ = 73.7 cm./sec.

For a constant-rate filtration in which the slurry consistency is less than 0.1%,

$$W/A = \rho s U (t - t_o) \qquad (10).$$

For the upper trace of Fig. 12,

$$s = 1.888/4150 = 0.000454 \text{ g./g.}$$

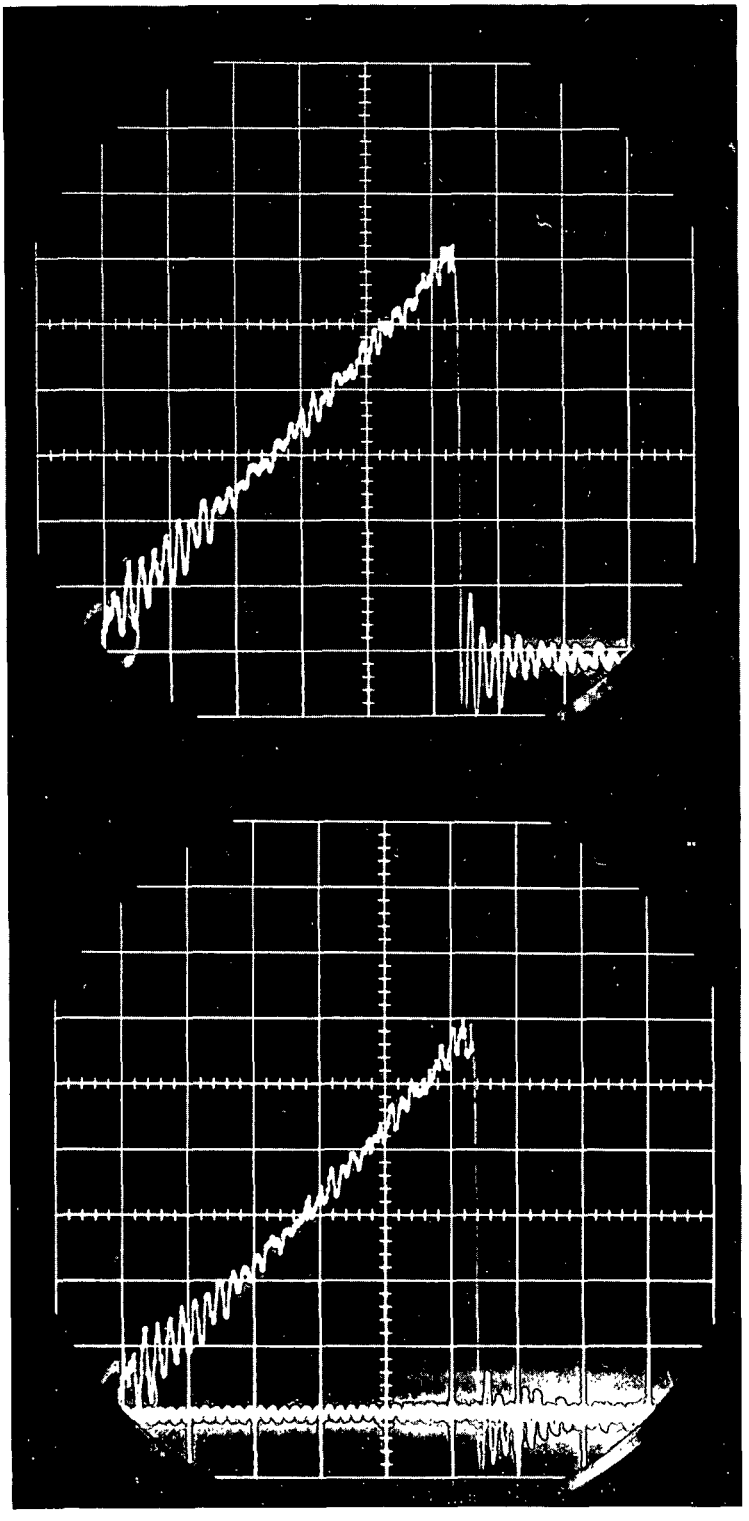

Figure 12. Pressure Trace of a Filtration Run

Horizontal scale: 0.2 sec./div.
Vertical scale: 40 cm. of water/div.

The horizontal or time scale is:

0.2 sec./large division (total run time = 1.05 sec.)

The vertical pressure scale is:

40 cm. H_2O/large division (max. pressure drop reached = 240 cm. H_2O)

The trace gives the <u>total</u> pressure drop-time curve for the filtration. This is composed of the pressure drops across the mat and the wire. The pressure drop across the mat is computed by subtracting the measured pressure drop across the wire alone (at the appropriate velocity) from the total.

In general, the filtration time must also be corrected because it is very difficult to start the filtration and the oscilloscope trace at exactly the same time. In this particular case, good synchronization was achieved and no correction is necessary. In case the filtration and oscilloscope are not synchronized exactly, the procedure for correcting the filtration times is to plot pressure drop (across the mat only) <u>vs</u>. time, extrapolate the curve to zero pressure, determine the time, $\underline{t}_o$, at zero pressure and subtract this value from the raw time data. Because of this extrapolation, there is in general an uncertainty of about $\pm$0.005 second in the filtration time.

A conventional 52 by 52-mesh wire screen was used in the filtration, and at a velocity of 73.7 cm./sec. the pressure drop across this screen was 16 cm. of water. Using this value, the slurry consistency, and calibration factors given previously, the following table was prepared from the upper trace of Fig. 12.

TABLE III

EXPERIMENTAL HIGH-VELOCITY FILTRATION DATA

Filtration Time, sec.	Total ΔH, cm. H_2O	Corr. ΔH, cm. H_2O	$W/A \times 10^4$, g./sq. cm.	$\Delta P \times 10^{-3}$, dynes/sq. cm.
0.20	60	44	67	43
0.40	98	82	132	80
0.60	140	124	202	122
0.80	186	170	269	167
1.00	232	216	336	212

These results and those prepared from the lower trace (a duplicate run) have been included in Fig. 7. The slurry consistency for the lower trace was

$s = 1.827/4150 = 0.0000439$ g./g.